IEEE Access
Multidisciplinary ⋮ Rapid Review ⋮ Open Access Journal

Received 14 May 2024, accepted 21 June 2024, date of publication 24 June 2024, date of current version 5 July 2024.

Digital Object Identifier 10.1109/ACCESS.2024.3418986

RESEARCH ARTICLE

Optimal Multi-Tooth Numbers for Vernier PM Synchronous Machines

YINZHAO ZHENG, ZI-QIANG ZHU, (Fellow, IEEE), HAI XU, (Graduate Student Member, IEEE), JUN YAN, AND DAWEI LIANG, (Member, IEEE)

Department of Electronic and Electrical Engineering, The University of Sheffield, S1 3JD Sheffield, U.K.

Corresponding author: Zi-Qiang Zhu (z.q.zhu@sheffield.ac.uk)

ABSTRACT This paper systematically investigates the effect of multi-tooth numbers on electromagnetic performances of conventional and consequent-pole (CP) vernier permanent magnet (PM) synchronous machines (VPMSMs), including average torque, overload capability, PM utilization, loss, efficiency, and power factor, etc. In particular, the influence of multi-tooth numbers on the unipolar end leakage flux of CP VPMSMs is investigated for the first time. It confirms that CP rotor and multi-tooth stator structures exhibit better field modulation effects compared with conventional north-south pole and non-multi-tooth stator structures. It reveals that there exists an optimal multi-tooth number for torque output capability and PM utilization, as well as unipolar end leakage flux. In particular, it shows that the multi-tooth stator structure helps save PM volume significantly for CP VPMSMs and suppress unipolar end leakage flux. The PM utilization rate of CP VPMSM with 5 multi-teeth is more than 50% higher than that with single-tooth structure while the unipolar end leakage flux is reduced by around 60%. However, the overload capability and power factor will be sacrificed. Finally, the prototypes with 2 and 3 multi-teeth numbers are manufactured and tested to verify the FEA analyses.

INDEX TERMS Consequent pole, field modulation, multi-tooth, permanent magnet, PM utilization, unipolar end leakage, vernier machine.

I. INTRODUCTION

Vernier permanent magnet synchronous machines (VPMSMs) become more popular in low-speed and high-torque applications due to their high torque density, high PM utilization, and relatively simple structure [1], [2], [3], [4]. Vernier machines (VMs) can be divided into overlapping winding open-slot stator VMs and non-overlapping concentrated winding multi-tooth stator VMs in terms of stator and armature winding configurations. According to rotor topologies, there are CP and north-south pole (NSP) structures [5]. For multi-tooth stator VMs, the stator tooth is split into several dummy slots to produce multipole effect. Together with non-overlapping fractional slot concentrated winding (FSCW), VMs with multi-tooth stator structures have the advantages of short axial end winding, high torque/power density, high efficiency, and enhanced flux weakening capability compared with their overlapping winding counterparts [6], [7], [8], [9], [10]. Furthermore, PM utilization and torque output capability can be enhanced when combined with a CP rotor structure [4], [11].

The torque characteristics of NSP surface-mounted PM (SPM) VMs with different stator slots and multi-tooth numbers are investigated and the optimal multi-tooth number is determined [12], [13], [14], [15], [16]. The coding shaped tooth NSP VPMSM that can increase average torque and reduce torque ripple compared with regular multi-tooth VMs is proposed [17]. However, the optimal multi-tooth numbers for CP VMs have not been investigated in [12], [13], [14], [15], and [16].

The CP structure can reduce around 30-40% of PM volume in FSCW SPM synchronous machines, but the average torque will be slightly reduced [4], [18]. However, the CP structure helps to reduce PM volume and increase the average torque simultaneously for interior PM (IPM) synchronous machines [11], [19]. The field modulation effects between

The associate editor coordinating the review of this manuscript and approving it for publication was Zhuang Xu.

NSP and CP structures are compared, which shows that the CP structure can generate higher modulated torque [20], [21]. The field modulation effect of different stator slot structures on NSP and/or CP PM machines is investigated [22], [23], [24], and the results show that the slot-opening ratio has a great influence on the field modulation effect. Field modulation effects and torque components of CP VPMSMs with 2 multi-teeth are investigated in [25], [26], [27], [28], and [29] which shows that the torque output capacity can be enhanced compared with conventional NSP VMs and single-tooth stator VMs.

The CP rotor structure leads to unipolar end leakage flux which will threaten the safety of the machine system. The unipolar end leakage flux in CP PM machines is investigated in [30], [31], [32], [33], [34], [35], [36], and [37], but few papers focus on CP VPMSMs [33], [34], [35]. The stator with 4-multi-teeth is proposed to suppress the magnetic unbalance caused by CP rotor structure [33]. Two conventional CP structures with opposite polarities are combined to reduce the unipolar end leakage in CP VPMSMs [34]. A simple composite rotor structure is proposed in [35] to eliminate the unipolar end leakage in CP VPMSMs.

However, the effect of different multi-tooth numbers on the electromagnetic performance, as well as unipolar end leakage flux, of CP VPMSMs has not been systematically investigated so far and will be the subject of this paper.

The main contributions of this paper can be summarized as follows: 1) The optimal multi-tooth number, in terms of torque characteristics, PM utilization, and efficiency, etc., is determined. It reveals that the CP rotor combined with multi-tooth stator structure has better field modulation effect and helps to increase torque output capability and improve PM utilization. However, the efficiency at higher speeds, power factor, and overload capability will be sacrificed while using the CP rotor and multi-tooth stator. 2) The electromagnetic performances of NSP and CP VPMSMs with different multi-tooth numbers are compared. The CP rotor has better average torque output capability and PM utilization, but higher cogging torque, poorer overload capability, and lower power factor compared with the NSP rotor. 3) The influence of critical design parameters of multi-tooth CP VPMSMs is investigated. It is found that the field modulation effect and torque output capability are very sensitive to the dimensions of multi-tooth and PMs. 4) The effect of different multi-tooth numbers on the unipolar end leakage flux is investigated for the first time, which reveals that the multi-tooth structure helps to suppress the unipolar end leakage flux, with around 60% reduction for CP VPMSM with 5 multi-teeth compared with that with single-tooth.

This paper is organized as follows. Machine topologies of 6-slot VPMSMs with different multi-tooth numbers and rotor topologies (CP and NSP) are presented in Section II. Then, in Section III, all machines are optimized for maximum average torque with the same active lamination stack length and fixed copper loss considering end-winding. The effect of multi-tooth numbers on electromagnetic performances of VPMSMs, including torque characteristics, PM utilization, loss, efficiency, etc., are investigated in Section IV. Section V analyses the influence of critical design parameters on field modulation effect and torque output capability while the unipolar end leakage flux of VPMSMs with different multi-tooth numbers is investigated in Section VI. Prototypes with different stator structures (2 and 3 multi-teeth numbers) and rotor topologies (NSP and CP) are manufactured and tested to verify the FEA analysis in Section VII and this paper is concluded in Section VIII.

II. MACHINE TOPOLOGIES

Vernier machines with multi-tooth stators and FSCWs have short end windings, which can achieve compact structure and higher torque density. The cross-sections of 6-slot FSCW VPMSMs with different multi-tooth numbers and rotor topologies (NSP and CP), i.e., 6-slot/1-tooth/8-pole (6s/1t/8p), 6-slot/2 multi-teeth/20-pole (6s/2mt/20p), 6-slot/3 multi-teeth/32-pole (6s/3mt/32p), 6-slot/4 multi-teeth/44-pole (6s/4mt/44p), and 6-slot/5 multi-teeth/56-pole (6s/5mt/56p) FSCW VPMSMs, are illustrated in FIGURE 1. It should be noted that the conventional stator without multi-tooth structure, as shown in FIGURE 1 (a), is named 1-tooth in this paper for convenience.

For VMs, the relationship between stator slot number (Z_s), armature winding pole pair number (P_a), and rotor pole pair number (P_r) should satisfy:

$$Z_s = P_r \pm P_a \tag{1}$$

For VMs with n_{st}-multi-teeth in stator big tooth (Z_s), the relationship should be

$$n_{st} Z_s = P_r \pm P_a \tag{2}$$

The analytical method is used to reveal field modulation and magnetic gearing effects. Magnetic saturation, magnetic leakage, end-effect, and fringing effect are neglected to simplify the analysis.

The magnetomotive force (MMF) of rotating PMs can be expressed as

$$F_{PM}(\theta, t) = \sum_{i=1}^{\infty} A_{PMi} \cos\left(i p_r (\theta - \omega t)\right) \tag{3}$$

where p_r is the pole-pair number of rotor PMs, ω is the electrical velocity, θ is the mechanical angle, and A_{PMi} is the magnitude of i^{th} order harmonic.

For the NSP rotor,

$$A_{PMi} = \frac{4 B_r h_{PM}}{i \mu_0 \mu_r \pi} \sin\left(\frac{i\pi}{2}\right) \sin\left(\frac{i p_r \theta_{PM}}{2}\right) \tag{4}$$

For the CP rotor,

$$A_{PMi} = \frac{4 B_r h_{PM}}{i \mu_0 \mu_r \pi} \sin\left(\frac{i p_r \theta_{PM}}{2}\right) \tag{5}$$

where B_r, h_{PM}, μ_r, and θ_{PM} are the remanence, the thickness, the relative permeability, and the pole arc of rotor PMs, respectively.

The air-gap permeance accounting for the stator slots can be expressed as

$$\Lambda_s(\theta) = \Lambda_{s0} + \sum_{j=1}^{\infty} \Lambda_{sj} \cos(jZ_s\theta + \pi) \tag{6}$$

When slot pitches of multi-tooth are equal, Z_s is replaced by $n_{st}Z_s$, which is the total stator multi-tooth numbers, i.e., 12 and 18 in FIGURES 1 (b) and (c). n_{st} is the multi-tooth number per stator-tooth.

The open-circuit air-gap flux density is

$$\begin{aligned} B_m(\theta,t) &= F_{PM}(\theta,t)\,\Lambda_s(\theta) \\ &= \Lambda_{s0} * \sum_{i=1}^{\infty} A_{PMi}\cos[ip_r(\theta-\omega t)] \\ &\quad + \frac{1}{2}\sum_{i=1}^{\infty}\sum_{j=1}^{\infty} \Lambda_{sj}A_{PMi}\cos[(ip_r \pm jp_s)\theta - ip_r\omega t] \end{aligned} \tag{7}$$

The pole-pair number of armature winding should satisfy $p_a = n_{st}Z_s - p_r$ for achieving high torque [27]. The back-EMF induced by the rotor PM magnetic field is

$$\begin{aligned} e_A(t) &= -\frac{d}{dt}\lambda_{PM}(t) \\ &= -\frac{d}{dt}[r_\delta l_{ef} n_c \int_0^{\frac{2\pi}{Z_s}} B_m(\theta,t)\,d\theta] = \omega r_\delta l_{ef} n_c \\ &\quad \times \{\Lambda_{s0}\sum_{i=1}^{\infty} A_{PMi}[cos(ip_r\frac{2\pi}{Z_s} - ip_r\omega t) - \cos(ip_r\omega t)] \\ &\quad + \frac{1}{2}\sum_{i=1}^{\infty}\sum_{j=1}^{\infty}\frac{ip_r}{ip_r \pm jZ_s}\Lambda_{sj}A_{PMi} \\ &\quad \times [\cos((ip_r \pm jZ_s)\theta - ip_r\omega t) - \cos(ip_r\omega t)]\} \end{aligned} \tag{8}$$

where r_δ is the air-gap radius, l_{ef} is the axial length of stator lamination, and n_c is the number of turns per coil.

To simplify the analysis, higher order harmonics are neglected due to their low amplitudes. Only considering $i = 1, j = 1$ or n_{st}, and $ip_r - jZ_s$ in $ip_r \pm jZ_s$, the back-EMF can be rewritten as

$$\begin{aligned} &e_A(t) \\ &= \omega r_\delta l_{ef} n_c[\cos(p_a\frac{2\pi}{Z_s} + p_r\omega t) - \cos(p_r\omega t)] \\ &\quad \times (\Lambda_{s0}A_{PM1} + \frac{1}{2}\frac{p_r}{p_r - N_s}\Lambda_{s1}A_{PM1} - \frac{1}{2}\frac{p_r}{p_a}\Lambda_{sn_{st}}A_{PM1}) \end{aligned} \tag{9}$$

The back-EMF contains EMFs generated by unmodulated and modulated field components. The first term is generated by the unmodulated field. The second term is generated by the field modulation effect of stator big tooth (Z_s) while the third term is generated by the field modulation effect of multi-tooth ($n_{st}Z_s$).

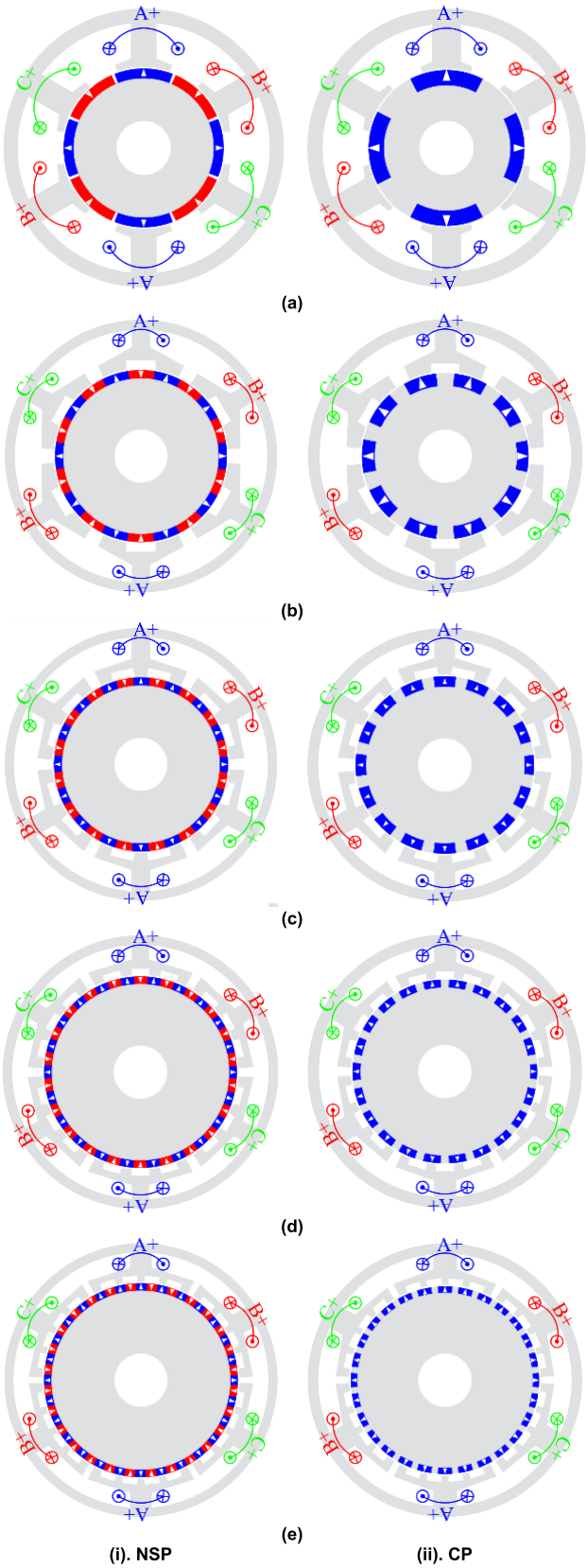

FIGURE 1. Machine topologies of 6-slot FSCW VPMSMs with different multi-tooth numbers and rotor topologies. (a) 6s/1t/8p. (b) 6s/2mt/20p. (c) 6s/3mt/32p. (d) 6s/4mt/44p. (e) 6s/5mt/56p.

When three-phase sinusoidal current and $i_d = 0$ control is applied, the average electromagnetic torque is expressed as:

$$T_{av} = \frac{3E_A I_A}{2\omega} = \frac{3}{2} I_A r_\delta l_{ef} n_c (\Lambda_{s0} A_{PM1} + \frac{1}{2} \sum_{j=1}^{\infty} \frac{p_r}{p_r \pm jZ_s} \Lambda_{sj} A_{PM1}) \quad (10)$$

The average electromagnetic torque can be simplified as:

$$T_{av} = \frac{3}{2} I_A r_\delta l_{ef} n_c \times (\Lambda_{s0} A_{PM1} + \frac{1}{2} \frac{p_r}{p_r - Z_s} \Lambda_{s1} A_{PM1} - \frac{1}{2} \frac{p_r}{p_a} \Lambda_{sn_{st}} A_{PM1}) \quad (11)$$

III. MACHINE OPTIMIZATION

The 6-slot VPMSMs with different multi-tooth numbers (one to five) and rotor topologies (NSP and CP) are globally optimized for maximum average torque under fixed 40 W copper loss considering end winding. During the optimization, fixed parameters are listed in Table 1, including stator outer diameter (100 mm), active stack length (50 mm), air-gap length (1 mm), shaft diameter (20 mm), and copper loss considering end winding (40 W). Stator inner radius (r_{si}), yoke thickness (h_y), tooth width (w_t), slot opening height (h_{s0}), stator slot opening width (b_{s0}), width of multi-tooth and depth of dummy slot (w_{mt} and $h_{mt}(w_{mt1} = w_{mt2})$), and pole arc to pole pitch ratio of rotor PM (p_{rPM}) will be globally optimized as shown in FIGURE 2. The p_{rPM} is defined as θ_{pm}/θ_1.

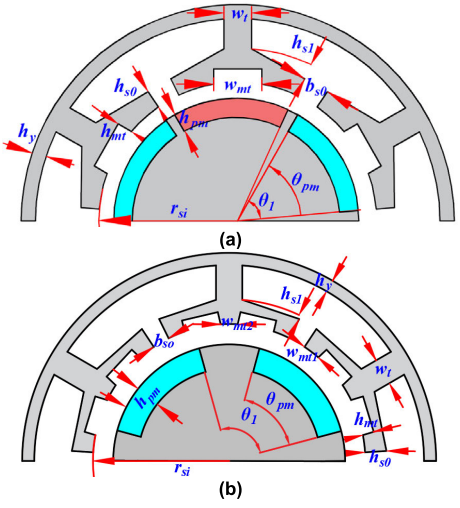

FIGURE 2. Illustration of variables of 6-slot VPMSMs during the optimization. (a) NSP with 2mt. (b) CP with 3mt.

For NSP VPMSMs, the PM volume is fixed at 24.5 cm^3 while two scenarios are considered for CP VPMSMs, i.e., fixed 24.5 cm^3 PM volume and unfixed PM volume.

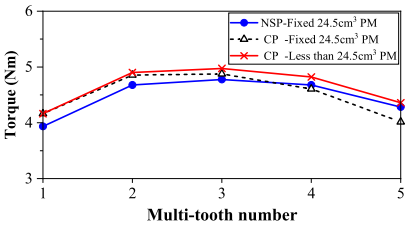

FIGURE 3. Optimized torques of 6-slot VPMSMs with different multi-tooth numbers and rotor topologies.

TABLE 1. Fixed parameters of NSP and CP VPMSMs.

Parameters	Unit	Value
Number of stator slot (Z_s)	-	6
Number of rotor pole ($2p$)	-	8/20/32/44/56
Stator outer diameter (d_{so})	mm	100
Active stack length (l_{fe})	mm	50
Number of turns per phase (N_{ph})	-	184
Slot filling factor (s_f)	-	0.28
Air-gap length (δ)	mm	1
Shaft diameter (d_{sh})	mm	20
PM remanence (B_r)	T	1.20
PM relative permeability (μ_r)	-	1.05

TABLE 2. Optimized variables of NSP VPMSMs.

Parameters	Unit	Value				
Multi-tooth	-	1	2	3	4	5
r_{si}	mm	29.45	32.07	32.47	35.95	36.44
h_y	mm	4.62	3.30	3.05	3.07	2.89
w_t	mm	8.86	6.40	6.01	5.96	7.40
b_{s0}	mm	11.72	10.37	10.55	10.29	11.83
h_{s0}	mm	1.98	4.21	5.22	5.04	4.62
w_{mt1}	mm	-	8.57	4.13	3.42	2.36
h_{mt}	mm	-	3.40	2.52	2.34	2.16
h_{PM}	mm	3.11	2.66	2.63	2.36	2.32
V_{PM}	cm^3	24.5	24.5	24.5	24.5	24.5
p_{rPM}	-	0.932	0.986	0.985	0.980	0.982
T_{av}	Nm	3.94	4.68	4.78	4.68	4.28
T_{ripple}	%	14.91	7.23	6.97	3.70	2.86
I_{peak}	A	5.60	5.14	5.19	4.31	4.24

TABLE 3. Optimized Variables of CP VPMSMs.

Parameters	Unit	Value				
Multi-tooth	-	1	2	3	4	5
r_{si}	mm	28.92	31.30	33.42	34.90	35.21
h_y	mm	5.40	3.76	3.51	3.46	3.45
w_t	mm	10.03	7.28	7.10	7.24	9.16
b_{s0}	mm	1.63	4.77	5.51	4.80	4.57
h_{s0}	mm	12.80	6.15	4.91	4.10	2.67
w_{mt1}	mm	-	7.85	3.99	2.80	2.51
h_{mt}	mm	-	3.37	2.78	2.74	1.72
h_{PM}	mm	5.07	4.28	3.44	2.84	2.19
V_{PM}	cm^3	24.5	23.72	19.96	17.50	13.77
p_{rPM}	-	0.606	0.628	0.610	0.615	0.620
T_{av}	Nm	4.15	4.90	4.97	4.82	4.36
T_{ripple}	%	50.16	40.18	19.11	18.77	18.39
I_{peak}	A	5.54	5.14	4.61	4.29	4.13

FIGURE 3 compares the optimized torques of NSP and CP VPMSMs, where the optimized torque increases first and then decreases with the increase of multi-tooth number. When the PM volume for CP VPMSMs is fixed the same as that of NSP VPMSMs, the average torques of CP with

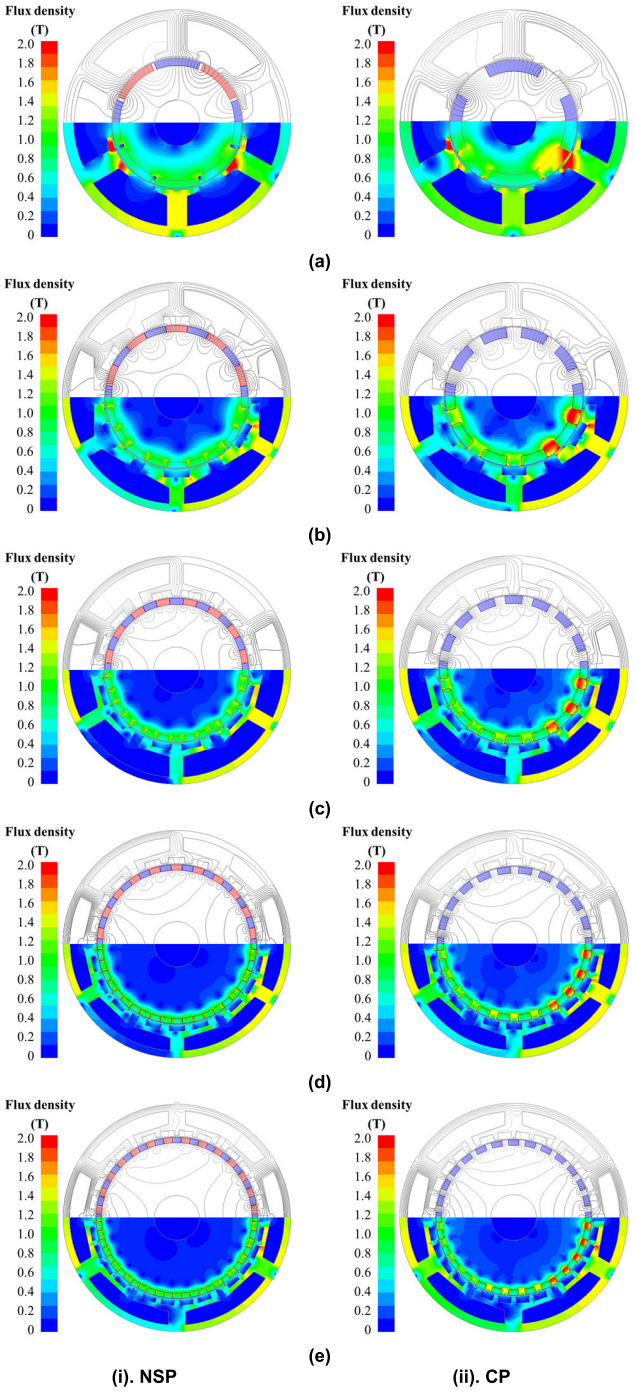

FIGURE 4. On-load magnetic field distributions of 6-slot VPMSMs with different multi-tooth numbers and rotor topologies. (a) 6s/1t/8p. (b) 6s/2mt/20p. (c) 6s/3mt/32p. (d) 6s/4mt/44p. (e) 6s/5mt/56p.

1-3 multi-tooth numbers are higher while the torques of CP with 4 and 5 multi-tooth numbers are lower than that of NSP counterparts. However, when PM volume is not fixed during optimization, the optimized torques of CP VPMSMs with different multi-tooth numbers will increase and always be higher than those of the corresponding NSP counterpart with any multi-tooth number. Moreover, the optimal PM volumes

TABLE 4. Comparison of PM volume, average torque, and PM utilization among CP VPMSMs with different multi-tooth numbers.

Multi-tooth number	PM volume (cm^3)	Average torque (Nm)	PM utilization (Nm/cm^3)
1	24.50	4.16	0.17
2	23.72	4.90	0.21
3	19.96	4.98	0.25
4	15.73	4.84	0.28
5	12.31	4.34	0.32

of CP VPMSMs with different multi-tooth numbers are less than 24.5 cm^3. The optimized CP VPMSMs with less than 24.5 cm^3 PM volume are chosen to be analyzed in this paper. Optimal parameters are listed in Table 2 (NSP) and Table 3 (CP). Meanwhile, optimal machine structures and on-load magnetic field distributions under 40 W copper loss are shown in FIGURE 4.

IV. COMPARISON OF ELECTROMAGNETIC PERFORMANCES

A. OPEN-CIRCUIT

The electromagnetic performances of optimized NSP and CP VPMSMs are compared in this section, including torque characteristics, PM utilization, efficiency, power factor, overload capability, etc.

Open-circuit radial air-gap flux densities, back-EMFs, and their FFT spectra of optimized 6-slot NSP and CP VPMSMs with different multi-tooth numbers are shown in FIGURE 5. NSP structures have higher fundamental components of open-circuit radial air-gap flux density but CP structures have higher modulated field harmonics as shown in FIGURE 5 (c), which means CP structures have better field modulation effects and have potential to generate higher back-EMFs. Fundamental components of open-circuit radial air-gap flux density decrease with the increase of multi-tooth number for both NSP and CP VPMSMs. However, due to the field modulation effect, fundamental components of open-circuit back-EMFs show different trends, increasing first and then decreasing. For both NSP and CP VPMSMs, the fundamental components of back EMF reach their maximum when the multi-tooth number is four.

B. TORQUE CHARACTERISTICS

FIGURES 6 and 7 show the torque characteristics of optimized 6-slot NSP and CP VPMSMs with different multi-tooth numbers. Average torques of CP VPMSMs with different multi-tooth numbers show the same trend as that of NSP VPMSMs, increasing first and then decreasing with the increase of multi-tooth numbers. The optimal multi-tooth numbers for maximum average torque under 40 W copper loss and 50 mm lamination stack length are three for both NSP and CP structures. The cogging torque and torque ripple decrease with the increase of multi-tooth number. The average torque of the CP structure is higher than that of the NSP counterpart, but the torque ripple and cogging torque are higher. The multi-tooth structure helps to reduce cogging

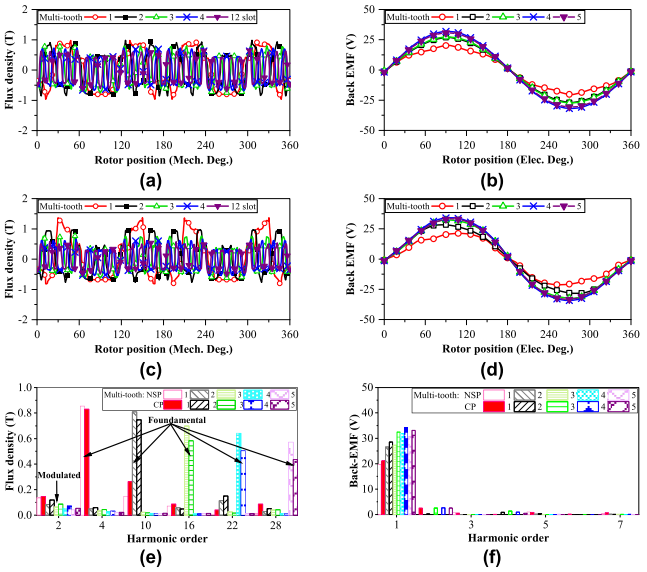

FIGURE 5. Open-circuit radial air-gap flux densities and back-EMFs of 6-slot NSP and CP VPMSMs with different multi-tooth numbers. (a) Air-gap flux densities of NSP. (b) Back-EMFs of NSP. (c) Air-gap flux densities of CP. (d) Back-EMFs of CP. (e) FFT spectra of air-gap flux density. (f) FFT spectra of back-EMF.

torque and torque ripple. Moreover, multi-tooth stator and CP rotor structures have poor overload capabilities as shown in FIGURE 7.

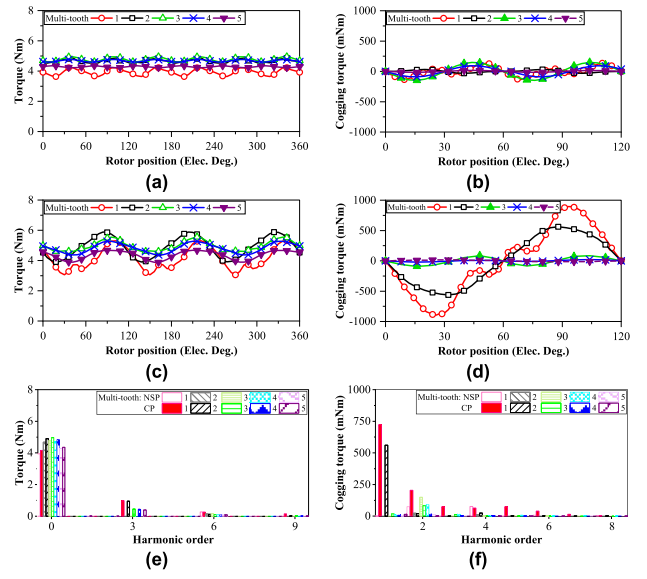

FIGURE 6. On-load torques and cogging torques of 6-slot NSP and CP VPMSMs with different multi-tooth numbers. (a) On-load torques of NSP. (b) Cogging torques of NSP. (c) On-load torques of CP. (d) Cogging torques of CP. (e) FFT spectra of on-load torque. (f) FFT spectra of cogging torque.

FIGURE 8 shows the average torque, torque ripple, and PM utilization comparison between optimized 6-slot NSP and CP VPMSMs with different multi-tooth numbers. It shows that the CP rotor combined with multi-tooth stator structure can help to reduce the PM volume and increase the

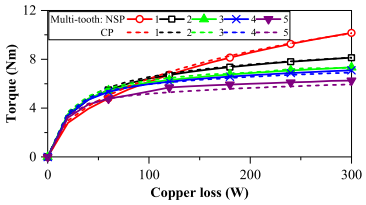

FIGURE 7. Overload capabilities of 6-slot NSP and CP VPMSMs with different multi-tooth numbers.

PM utilization. For CP structure, the optimal PM volume decreases with the increase of multi-tooth number. Thus, CP VPMSMs with higher multi-tooth numbers exhibit higher PM utilization. Especially for CP VPMSM with 5 multi-teeth, the PM volume is saved by about 50% compared with the corresponding NSP counterpart. Table 4 gives detailed data on average torque, PM usage, and PM utilization of CP VPMSMs with different multi-tooth numbers.

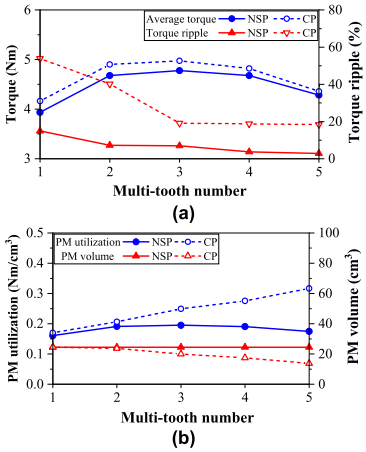

FIGURE 8. Average torques, torque ripples, and PM utilization comparison between optimized 6-slot CP and NSP VPMSMs with different multi-tooth numbers. (a) Average torque and torque ripple. (b) PM volume and PM utilization.

C. LOSS, EFFICIENCY, AND POWER FACTOR

FIGURE 9 shows losses, efficiencies, power factors, and d-axis inductances of optimized 6-slot NSP and CP VPMSMs under 40W copper loss and different speeds (400 and 1500 r/min). The iron loss increases with the increase of multi-tooth number while the PM loss shows the opposite trend because the PM volume per piece decreases when the multi-tooth number increases, leading to lower PM loss. The lower total PM volume of CP structure also causes lower total PM loss. As VPMSM with 3 multi-teeth has the highest average torque, it has higher efficiency at lower speed. When the speed increases, the iron loss increases with the increase of multi-tooth number, and thus, efficiency decreases with the increase of multi-tooth number at high speed conditions. The power factor decreases with the increase of multi-tooth number and the CP structure will further decrease the power

factor because the multi-tooth stator and CP rotor structures will increase the d-axis inductance.

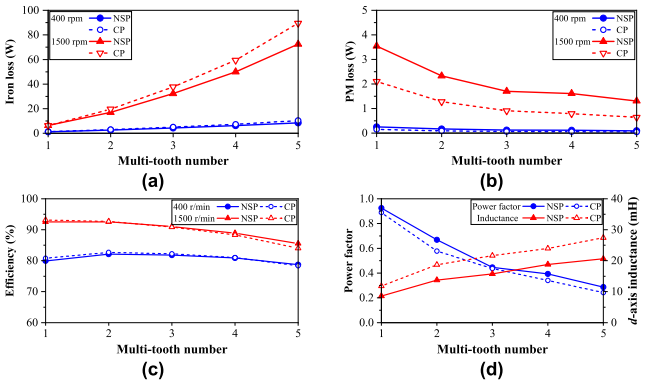

FIGURE 9. Losses, efficiencies, and power factors of optimized 6-slot CP and NSP VPMSMs with different multi-tooth numbers. (a) Iron loss. (b) PM loss. (c) Efficiency. (d) Power factor and d-axis inductance.

In conclusion, CP VPMSMs have higher torque output capability and higher efficiency at lower speed conditions (400 r/min) compared with their NSP counterparts. Moreover, the PM utilization will be improved significantly when combining the CP rotor and stator with higher multi-tooth numbers. About 50% of PM volume can be saved for CP VPMSM with 5 multi-teeth compared with the corresponding NSP counterpart. However, CP VPMSMs have lower power factor, much higher torque ripple and cogging torque, and poorer overload capability compared with their NSP counterparts.

V. INFLUENCE OF CRITICAL DESIGN PARAMETERS

In this section, the influence of critical design parameters on field modulation effect and average torque of CP VPMSMs is investigated, including the width of multi-tooth (w_{mt}) and the depth of dummy slot (h_{mt}) for the stator side and pole arc to pole pitch ratio and thickness of rotor PM (p_{rPM} and h_{PM}) for the rotor side as shown in FIGURE 10.

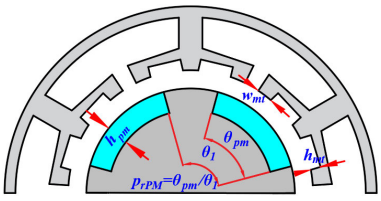

FIGURE 10. Illustration of critical parameters of CP VPMSMs.

A. WIDTH OF MULTI-TOOTH

The width of multi-tooth directly affects the equivalent air-gap permeance, and thus, affects the field modulation effect and average torque output capability of CP VPMSMs. FIGURE 11 shows the influence of width of multi-tooth on open-circuit air-gap flux density and average torque. The larger the multi-tooth width, the higher the equivalent air-gap permeance, and thus, the higher the fundamental component of open-circuit air-gap flux density. However, the modulated component of open-circuit air-gap flux density increases and then decreases with the increase of multi-tooth width. Consequently, the torque of CP VPMSMs is very sensitive to the width of multi-tooth. The multi-tooth width should be carefully selected to maintain fundamental air-gap flux density while achieving relatively higher modulated air-gap flux density to achieve maximum torque output capability. There is an optimal width for each CP VPMSM with different multi-tooth numbers.

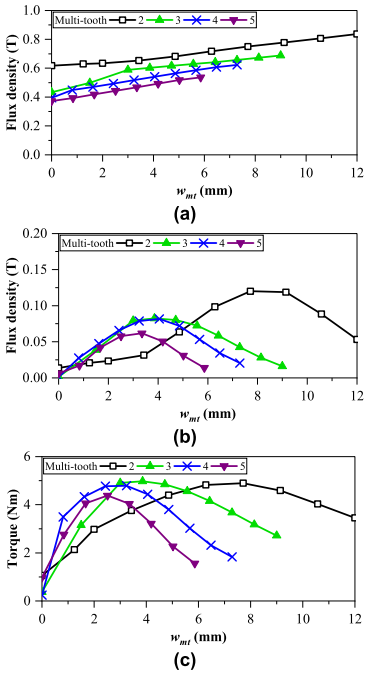

FIGURE 11. Influence of width of multi-tooth on air-gap flux density and average torque of CP VPMSMs. (a) Fundamental component of air-gap flux density. (b) Modulated component of air-gap flux density. (c) Torque.

B. DEPTH OF DUMMY SLOT

The influence of depth of dummy slot on open-circuit air-gap flux density and average torque of CP VPMSMs is shown in FIGURE 12. The increase of multi-tooth height will reduce the fundamental component of air-gap flux density while increasing the modulated component, showing that the height is also critical to the torque output capability. There exist optimal heights of multi-tooth numbers for different multi-tooth numbers, which decrease as multi-tooth numbers increase.

C. POLE ARC TO POLE PITCH RATIO

The PM dimensions affect the MMF of rotor PMs and the equivalent air-gap permeance of CP VPMSMs. Different from the pole arc to pole pitch ratio in NSP VPMSMs, which is usually 0.5, in CP VPMSMs the pole arc to pole pitch ratio can exceed 0.5 for better field modulation effect and torque output capability. FIGURE 13 shows the influence of pole

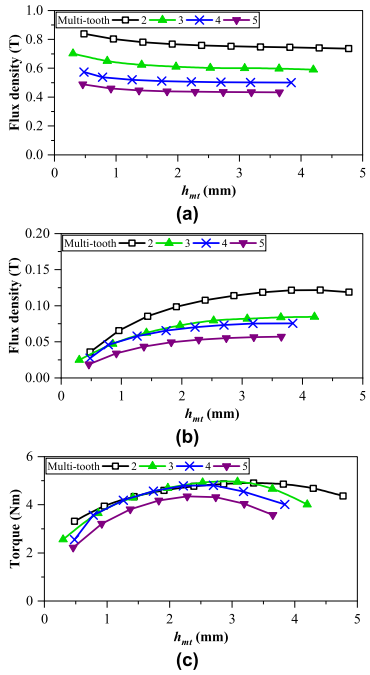

FIGURE 12. Influence of depth of dummy slot on air-gap flux density and average torque of CP VPMSMs. (a) Fundamental component of air-gap flux density. (b) Modulated component of air-gap flux density. (c) Torque.

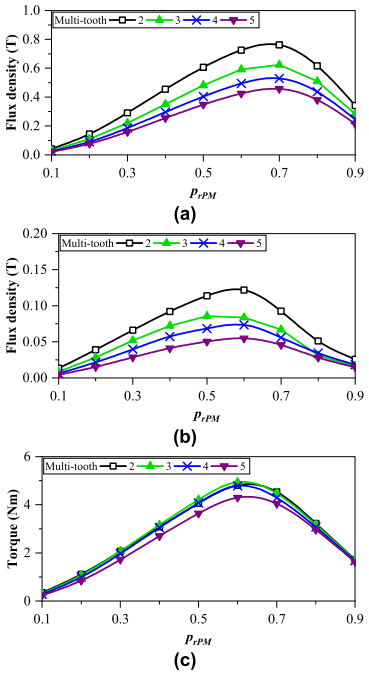

FIGURE 13. Influence of pole arc to pole pitch ratio of rotor PMs on air-gap flux density and average torque of CP VPMSMs. (a) Fundamental component of air-gap flux density. (b) Modulated component of air-gap flux density. (c) Torque.

arc to pole pitch ratio of rotor PMs on open-circuit air-gap flux density and average torque. Both the fundamental and modulated components of air-gap flux density increase and then decrease with the increase of pole arc to pole pitch ratio. For all CP VPMSMs, the maximum fundamental components are achieved at a pole arc to pole pitch ratio of 0.7, while the maximum modulated components are achieved at a pole arc to pole pitch ratio of 0.6. There is a trade-off between fundamental and modulated components of air-gap flux density for achieving maximum torque output, therefore, the optimal pole arc to pole pitch ratio of each CP VPMSM with different multi-tooth numbers is almost the same, between 0.60 and 0.63.

D. PM THICKNESS

The influence of rotor PM thickness on open-circuit air-gap flux density and average torque of CP VPMSMs is shown in FIGURE 14. The fundamental component of air-gap flux density increases first and then remains almost unchanged with the increase of PM thickness while the modulated component increases first and then decreases. As the PM thickness will affect the MMF of rotor PMs (5), flux leakage, and rotor core saturation, thicker PM does not guarantee higher average torque. The optimal PM thickness decreases significantly with the increase of multi-tooth number.

Overall, the field modulation effect and torque output capability are very sensitive to the dimensions of multi-tooth and PMs. The optimal width of multi-tooth and depth of dummy slot vary with the multi-tooth number. With the increase of multi-tooth number, the optimal PM thickness decreases significantly, while the optimal pole arc to pole pitch ratios are similar. Hence, the PM volume decreases with the increase of multi-tooth number.

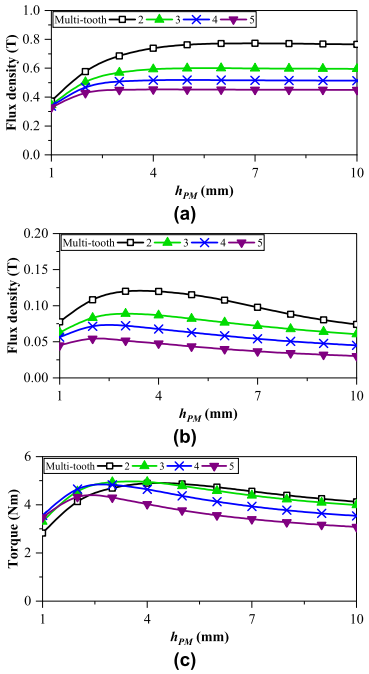

FIGURE 14. Influence of PM thickness on air-gap flux density and average torque of CP VPMSMs. (a) Fundamental component of air-gap flux density. (b) Modulated component of air-gap flux density. (c) Torque.

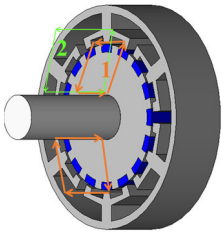

FIGURE 15. Magnetic paths of end leakage flux for CP VPMSM with 3 mt.

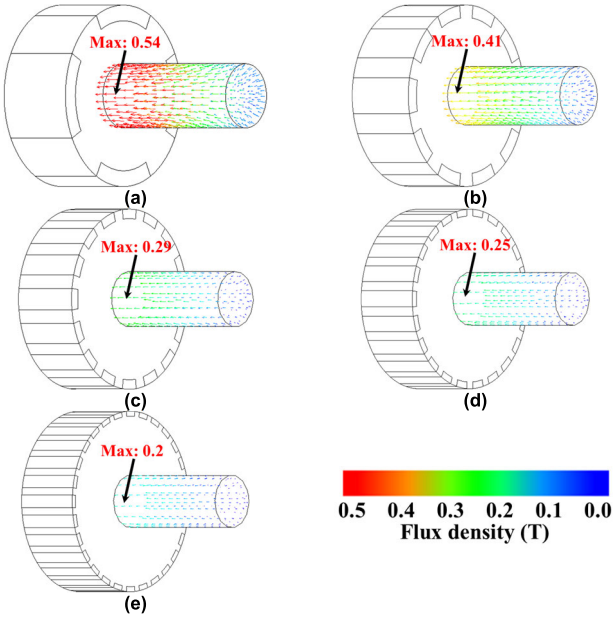

FIGURE 16. End leakage flux distributions of CP VPMSMs with magnetic shaft and different multi-tooth numbers under on-load condition with 40 W copper loss. (a) 1t. (b) 2mt. (c) 3mt. (d) 4mt. (e) 5mt.

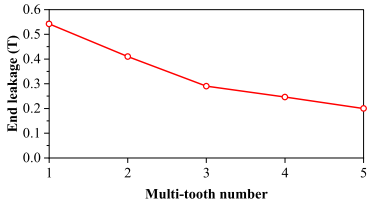

FIGURE 17. Maximum end leakage fluxes of VPMSMs on shaft surface.

VI. UNIPOLAR END LEAKAGE FLUX OF CP VPMSMS

Unbalanced magnetic circuits in the CP rotor structure lead to unipolar end leakage flux and magnetization on the shaft, which may threaten the safety operation of the machine system. The end leakage flux of CP VPMSMs with different multi-tooth numbers and rotor structures (conventional rotor with magnetic/non-magnetic shaft and composite rotor with non-magnetic/non-magnetic shaft) is investigated in this section.

A. UNIPOLAR END LEAKAGE FLUX DISTRIBUTION

3D FEA models are built to analyze end leakage flux distributions of CP VPMSMs with different multi-tooth numbers.

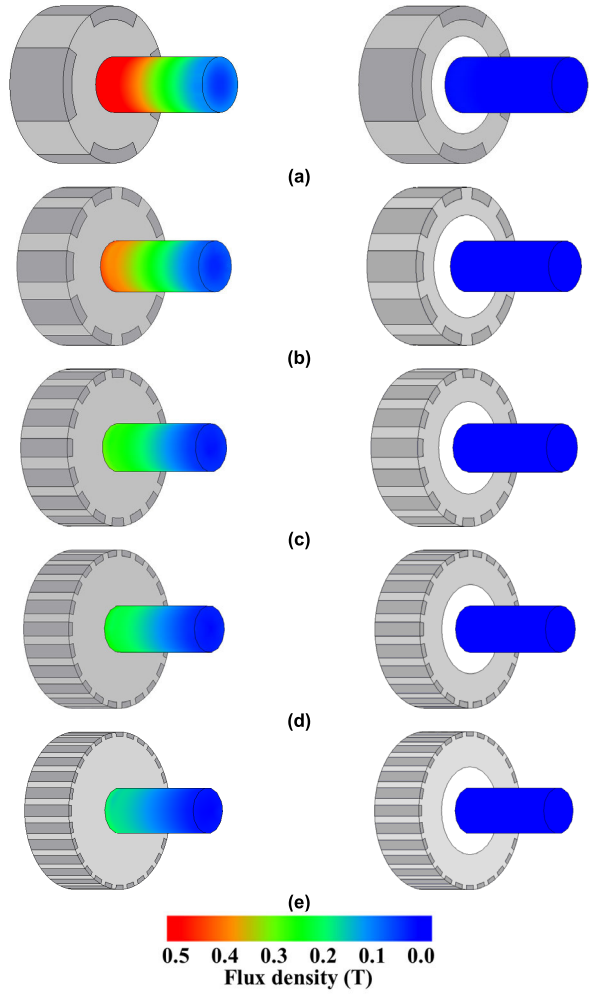

FIGURE 18. End leakage flux distributions of CP VPMSMs with different rotor structures under on-load condition with 40 W copper loss. (a) 1t. (b) 2mt. (c) 3mt. (d) 4mt. (e) 5mt.

TABLE 5. Key parameters of prototypes.

Parameters	Unit	Value	
Multi-tooth number	-	2	3
Stator inner radius (r_{si})	mm	32.0	33.5
Yoke thickness (h_y)	mm	3.4	3.5
Stator tooth width (w_t)	mm	6.6	7.0
Stator tooth tip height (h_{s0})	mm	4.4	5.64
Slot opening width (b_{s0})	mm	6.10	5.1
Multi-tooth width (w_{mtl})	mm	7.45	4.15
Multi-tooth height (h_{mt})	mm	3.64	3.0
PM height (h_{PM})	mm	4.0	4.0
Pole arc to pole pitch ratio (p_{rPM})	-	0.64	0.60
PM remanence (B_r)	T	1.20	
PM relative permeability (μ_r)	-	1.05	

Magnetic paths of end leakage flux for CP VPMSM with 3 multi-teeth are shown in FIGURE 15. The path with orange color is for end leakage caused by the PM magnetic field, while that with green color is for the armature reaction magnetic field. The unipolar end leakage flux is mainly caused by

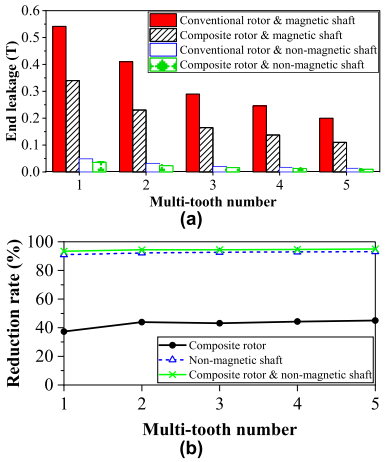

FIGURE 19. Comparison of maximum unipolar end leakage flux and reduction rate of CP VPMSMs with different rotor structures. (a) Maximum unipolar end leakage flux. (b) Reduction rate.

the PM magnetic field while the armature reaction only has a minor effect on end leakage flux because it will enhance the magnetic saturation [35].

End leakage flux distributions of CP VPMSMs with magnetic shaft (SUS430 magnetic stainless steel) and different multi-tooth numbers under on-load condition with 40 W copper loss are shown in FIGURE 16.

End leakage fluxes of all CP VPMSMs show significant unipolar distributions. FIGURE 17 shows the maximum end leakage fluxes of VPMSMs on the shaft surface about 3 mm away from the rotor end, which shows that the multi-tooth stator structure helps to reduce the end leakage flux and the higher the multi-tooth number, the lower the unipolar end leakage flux. The maximum end leakage flux of CP VPMSMs with 5 multi-teeth (6s/5mt/56p) is 0.20 T, more than 60% lower compared with VPMSMs without multi-tooth stator structure (6s/1t/8p), which is 0.54 T.

B. COMPOSITE ROTOR AND NON-MAGNETIC SHAFT

Inserting a non-magnetic ring between the rotor and shaft, forming a composite rotor structure, will increase the magnetic reluctance of end leakage flux path, thus, helping to reduce the unipolar end leakage flux while maintaining the average torque output capability, especially when non-magnetic shaft is used [35]. FIGURE 18 shows end leakage flux distributions of CP VPMSMs with different rotor structures under 40 W copper loss. The combination of composite rotor and non-magnetic shaft can reduce end leakage flux significantly.

FIGURE 19 shows the maximum unipolar end leakage flux and reduction rate of CP VPMSMs with different rotor structures. Compared with the conventional rotor, the composite rotor structure can reduce around 40% of the maximum end leakage flux while the composite rotor with non-magnetic shaft can reduce around 95% of the maximum end leakage flux.

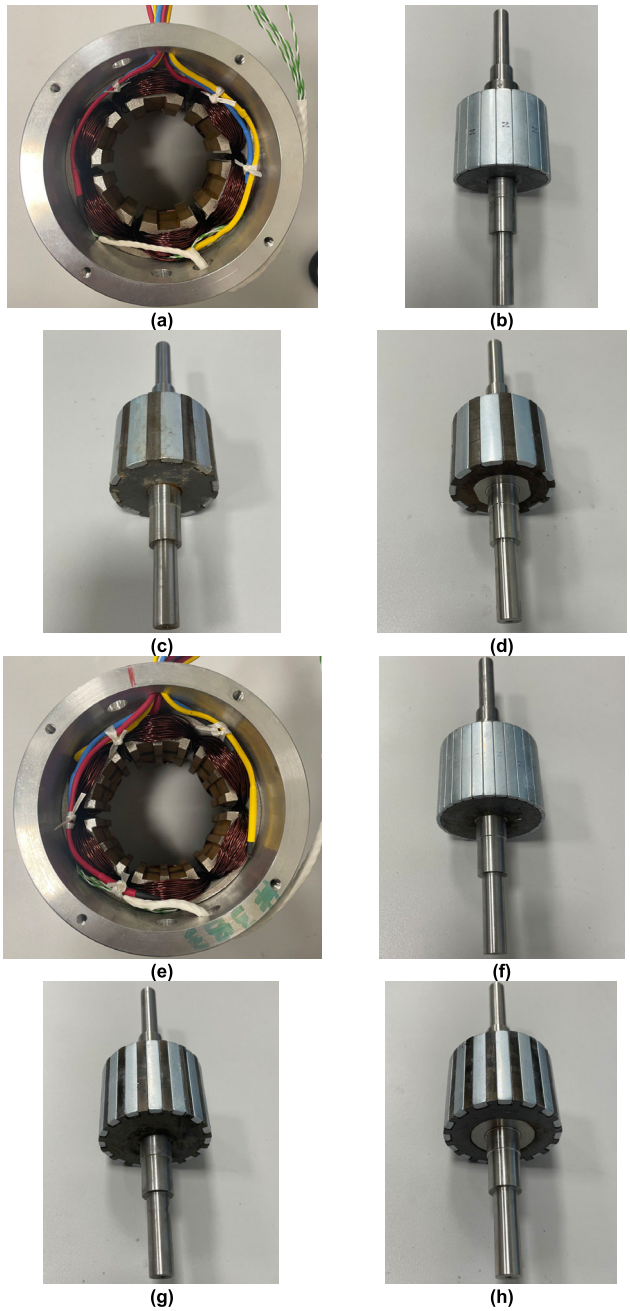

FIGURE 20. Prototype 6s/2mt/20p and 6s/3mt/32p VPMSMs. (a) 6s/2mt/20p stator. (b) 20p NSP rotor. (c) 20p CP conventional rotor with magnetic shaft. (d) 20p CP composite rotor with non-magnetic shaft. (e) 6s/3mt/32p stator. (f) 32p NSP rotor. (g) 32p CP conventional rotor with magnetic shaft. (h) 32p CP composite rotor with non-magnetic shaft.

VII. EXPERIMENTAL VALIDATION

A. ELECTROMAGNETIC PERFORMANCE

Two VPMSMs (6s/2mt/20p and 6s/3mt/32p) with NSP and CP rotors are prototyped. For the CP rotor, the conventional rotor with magnetic shaft (stainless steel SUS430) and the composite rotor with non-magnetic shaft (stainless steel SUS304) are manufactured. Prototypes are tested to verify the effectiveness of FEA analysis.

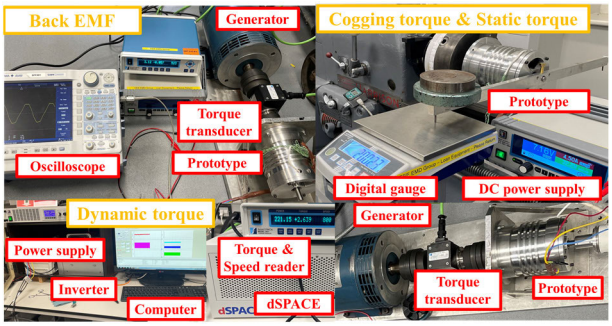

FIGURE 21. Test rigs for back EMF, cogging torque, static torque, and dynamic torque.

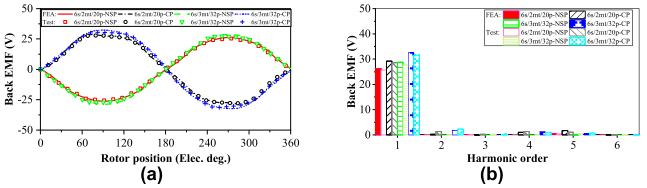

FIGURE 22. Measured and FEA predicted open-circuit back EMFs at 400 r/min. (a) Waveforms. (b). FFT spectra.

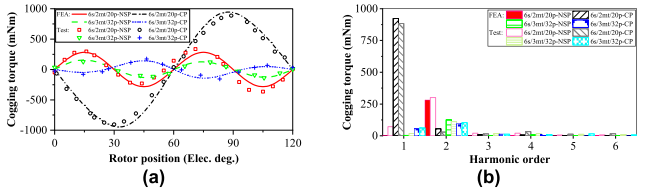

FIGURE 23. Measured and FEA predicted cogging torques. (a) Waveforms. (b). FFT spectra.

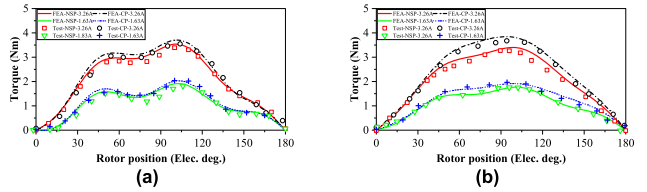

FIGURE 24. Measured and FEA predicted static torques. (a) 6s/2mt/20p. (b) 6s/3mt/32p.

FIGURE 20 shows stators, NSP rotors, CP conventional rotors, and CP composite rotors of prototypes. Table 5 lists the key parameters of prototypes. The test rigs for back EMF, cogging torque and static torque [38], and dynamic torque are shown in FIGURE 21.

FIGURE 22 shows measured and FEA predicted open-circuit back EMFs at 400 r/min which shows good agreement. VPMSMs with 3 multi-teeth have higher fundamental components of back EMF compared with 2 multi-teeth ones. CP rotor structure can also generate higher fundamental component of back EMF compared with its NSP counterpart.

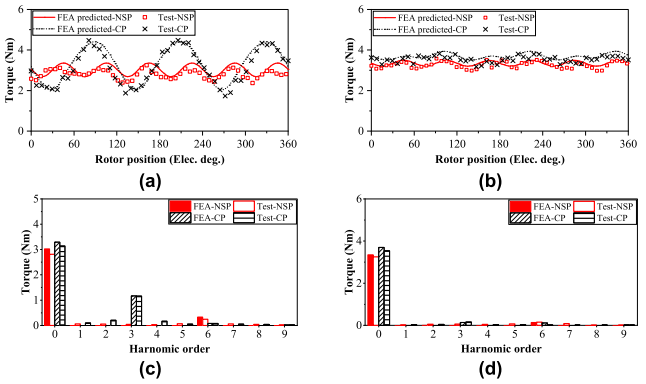

FIGURE 25. Measured and FEA predicted dynamic torques. (a) Dynamic torques of 6s/2mt/20p. (b) Dynamic torques of 6s/3mt/32p. (c) FFT spectra of dynamic torques of 6s/2mt/20p. (d) FFT spectra of dynamic torques of 6s/3mt/32p.

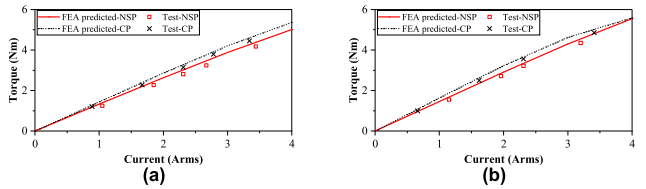

FIGURE 26. Measured and FEA predicted torque-current characteristics. (a) 6s/2mt/20p. (b) 6s/3mt/32p.

FIGURE 23 shows the measured and FEA-predicted cogging torques. VPMSMs with 3 multi-teeth have lower cogging torque compared with those with 2 multi-teeth while the CP rotor structure has higher cogging torque compared with its NSP counterpart.

The static torque is measured by injecting current through the DC power supply ($I_b = I_c = -0.5I_a$) and rotating the stator while keeping the rotor stationary, and then, the relationship between static torque and rotor position can be measured. Measured and FEA predicted static torques match well as shown in FIGURE 24. The static torque of CP VPMSM is slightly higher than that of the NSP counterpart.

Measured and FEA predicted dynamic torques match well as shown in FIGURE 25. FIGURE 26 shows measured and FEA predicted torque-current characteristics, which also shows good agreement.

B. UNIPOLAR END LEAKAGE

The unipolar end leakage flux of the whole shaft region can be measured with the bare rotor before assembling as shown in Figs 27, as well as the measured end leakage flux in the shaft region outside the end cap after assembling.

The unipolar end leakage fluxes of two machines before and after assembling with conventional rotor and magnetic shaft as well as with composite rotor and non-magnetic shaft obtained by FEA and measurements are compared in FIGURE 28. FEA-predicted results match well with the measurements. The 6s/3mt/32p VPMSM has lower end leakage flux than 6s/2mt/20p. In addition, employing

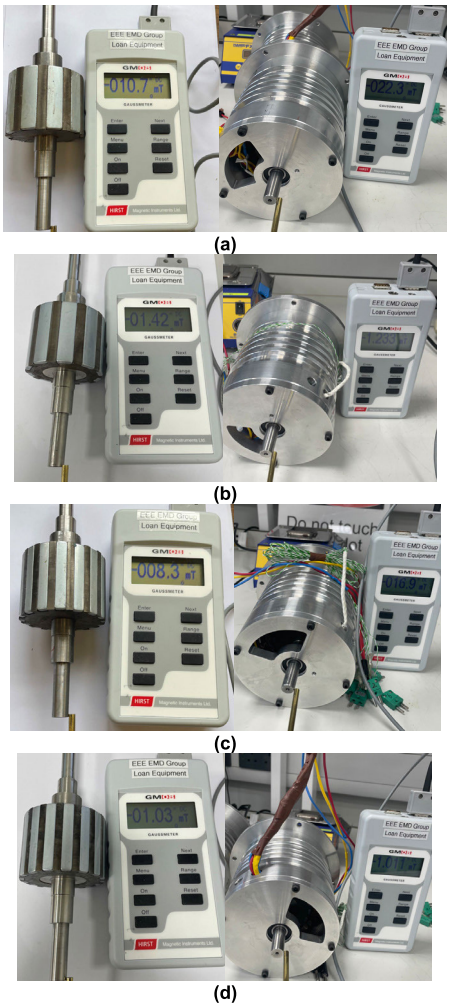

FIGURE 27. Illustration of measuring unipolar end leakage flux. (a) 6s/2mt/20p conventional rotor and magnetic shaft. (b) 6s/2mt/20p composite rotor and non-magnetic shaft. (c) 6s/3mt/32p conventional rotor and magnetic shaft. (d) 6s/3mt/32p composite rotor and non-magnetic shaft.

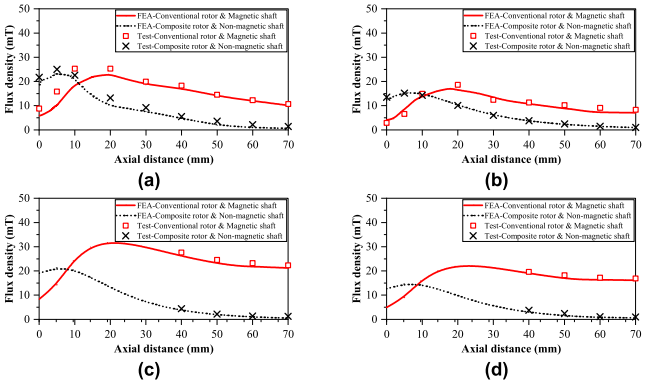

FIGURE 28. Measured and FEA predicted end leakage fluxes. (a) 6s/2mt/20p bare rotor. (b) 6s/3mt/32p bare rotor. (c) 6s/2mt/20p assembled. (d) 6s/3mt/32p assembled.

the non-magnetic ring and non-magnetic shaft effectively reduces the unipolar end leakage flux for both prototypes.

VIII. CONCLUSION

In this paper, the effect of multi-tooth number on electromagnetic performances of consequent-pole vernier PMSMs is investigated. Two prototypes are manufactured and tested to verify the FEA analysis. It confirms that the CP rotor combined with multi-tooth stator structure has better field modulation effect and helps to increase torque output capability and PM utilization. It reveals that there is an optimal multi-tooth number (3 for the analyzed machines) for maximizing average torque. With the increase of multi-tooth number, the PM utilization will be improved significantly (saved about 50% for 5 multi-teeth), but the efficiency at higher speeds, power factor, and overload capability will be sacrificed. Moreover, it has been found, for the first time, that the multi-tooth stator structure helps to reduce more than 60% of the maximum unipolar end leakage flux of CP VPMSMs compared with CP VPMSMs with single-tooth stator structure. In addition, the influence of critical design parameters of CP VPMSMs, which should be carefully selected to achieve better field modulation effect and maximum torque output capability, is investigated, including the width of multi-tooth and depth of dummy slot, the pole arc to pole pitch ratio, and the PM thickness.

REFERENCES

[1] A. Ishizaki, "Theory and optimum design of PM Vernier motor," in *Proc. 7th Int. Conf. Electr. Mach. Drives*, 1995, pp. 208–212.

[2] T. A. Lipo and A. Toba, "Generic torque-maximizing design methodology of surface permanent-magnet Vernier machine," *IEEE Trans. Ind. Appl.*, vol. 36, no. 6, pp. 1539–1546, Nov. 2000.

[3] S.-U. Chung, J.-M. Kim, D.-H. Koo, B.-C. Woo, D.-K. Hong, and J.-Y. Lee, "Fractional slot concentrated winding permanent magnet synchronous machine with consequent pole rotor for low speed direct drive," *IEEE Trans. Magn.*, vol. 48, no. 11, pp. 2965–2968, Nov. 2012.

[4] S.-U. Chung, J.-W. Kim, Y.-D. Chun, B.-C. Woo, and D.-K. Hong, "Fractional slot concentrated winding PMSM with consequent pole rotor for a low-speed direct drive: Reduction of rare earth permanent magnet," *IEEE Trans. Energy Convers.*, vol. 30, no. 1, pp. 103–109, Mar. 2015.

[5] A. Toba and T. A. Lipo, "Novel dual-excitation permanent magnet Vernier machine," in *Proc. IEEE Ind. Appl. Conf. 34th IAS Annu. Meeting*, Oct. 1999, pp. 2539–2544.

[6] A. M. El-Refaie, "Fractional-slot concentrated-windings synchronous permanent magnet machines: Opportunities and challenges," *IEEE Trans. Ind. Electron.*, vol. 57, no. 1, pp. 107–121, Jan. 2010.

[7] L. Xu, G. Liu, W. Zhao, J. Ji, H. Zhou, W. Zhao, and T. Jiang, "Quantitative comparison of integral and fractional slot permanent magnet Vernier motors," *IEEE Trans. Energy Convers.*, vol. 30, no. 4, pp. 1483–1495, Dec. 2015.

[8] B. Xu, Q. Wu, J. Ma, L. Wu, L. Qiu, X. Liu, and Y. Fang, "Research on the influence of end turn length on consequent-pole Vernier permanent-magnet machines," *IEEE Trans. Magn.*, vol. 58, no. 8, pp. 1–9, Aug. 2022.

[9] J. Li, K. T. Chau, J. Z. Jiang, C. Liu, and W. Li, "A new efficient permanent-magnet Vernier machine for wind power generation," *IEEE Trans. Magn.*, vol. 46, no. 6, pp. 1475–1478, Jun. 2010.

[10] S. L. Ho, S. Niu, and W. N. Fu, "Design and comparison of Vernier permanent magnet machines," *IEEE Trans. Magn.*, vol. 47, no. 10, pp. 3280–3283, Oct. 2011.

[11] L. Zhang, K. Wang, J. Li, and F. Li, "Comparison study of interior permanent magnet synchronous machine with conventional and consequent pole rotor," in *Proc. 22nd Int. Conf. Electr. Mach. Syst. (ICEMS)*, Aug. 2019, pp. 1–5.

[12] K. Okada, N. Niguchi, and K. Hirata, "Analysis of a Vernier motor with concentrated windings," *IEEE Trans. Magn.*, vol. 49, no. 5, pp. 2241–2244, May 2013.
[13] T. Zou, D. Li, R. Qu, D. Jiang, and J. Li, "Advanced high torque density PM Vernier machine with multiple working harmonics," *IEEE Trans. Ind. Appl.*, vol. 53, no. 6, pp. 5295–5304, Nov. 2017.
[14] H. Li, Z. Q. Zhu, and Y. Liu, "Optimal number of field modulation pole in Vernier permanent magnet synchronous machines," *IEEE Trans. Ind. Appl.*, vol. 55, no. 6, pp. 5747–5757, Nov./Dec. 2019.
[15] K. Xie, D. Li, R. Qu, X. Ren, M. R. Shah, and Y. Pan, "A new perspective on the PM Vernier machine mechanism," *IEEE Trans. Ind. Appl.*, vol. 55, no. 2, pp. 1420–1429, Mar. 2019.
[16] Y. Yu, F. Chai, Y. Pei, and L. Chen, "Comparisons of torque performance in surface-mounted PM Vernier machines with different stator tooth topologies," *IEEE Trans. Ind. Appl.*, vol. 55, no. 4, pp. 3671–3684, Jul. 2019.
[17] L. Fang, D. Li, X. Ren, and R. Qu, "A novel permanent magnet Vernier machine with coding-shaped tooth," *IEEE Trans. Ind. Electron.*, vol. 69, no. 6, pp. 6058–6068, Jun. 2022.
[18] J. Li and K. Wang, "Analytical determination of optimal PM-arc ratio of consequent-pole permanent magnet machines," *IEEE/ASME Trans. Mechatronics*, vol. 23, no. 5, pp. 2168–2177, Oct. 2018.
[19] L. Wu and R. Qu, "Comparison of conventional and consequent pole interior permanent magnet machines for electric vehicle application," in *Proc. 17th Int. Conf. Electr. Mach. Syst. (ICEMS)*, Oct. 2014, pp. 70–74.
[20] Y. Li, H. Yang, H. Lin, L. Qin, and S. Lyu, "Investigation of double-side field modulation mechanism in consequent-pole PM machines with concentrated windings," *IEEE Trans. Energy Convers.*, vol. 36, no. 3, pp. 1635–1648, Sep. 2021.
[21] Y. Gao, R. Qu, D. Li, J. Li, and G. Zhou, "Consequent-pole flux-reversal permanent-magnet machine for electric vehicle propulsion," *IEEE Trans. Appl. Supercond.*, vol. 26, no. 4, pp. 1–5, Jun. 2016.
[22] Z. Q. Zhu and Y. Liu, "Analysis of air-gap field modulation and magnetic gearing effect in fractional-slot concentrated-winding permanent-magnet synchronous machines," *IEEE Trans. Ind. Electron.*, vol. 65, no. 5, pp. 3688–3698, May 2018.
[23] D. Li, T. Zou, R. Qu, and D. Jiang, "Analysis of fractional-slot concentrated winding PM Vernier machines with regular open-slot stators," *IEEE Trans. Ind. Appl.*, vol. 54, no. 2, pp. 1320–1330, Mar. 2018.
[24] Y. Li, H. Yang, H. Lin, and Z. Zhao, "Comparative study of field modulation effects in consequent-pole PM machines with different stator slot configurations," *IEEE Trans. Magn.*, vol. 59, no. 11, pp. 1–6, Nov. 2023.
[25] G. Xu, G. Liu, M. Chen, X. Du, and M. Xu, "Cost-effective Vernier permanent-magnet machine with high torque performance," *IEEE Trans. Magn.*, vol. 53, no. 11, pp. 1–4, Nov. 2017.
[26] D. Jang and J. Chang, "Investigation of doubly salient structure for permanent magnet Vernier machines using flux modulation effects," *IEEE Trans. Energy Convers.*, vol. 34, no. 4, pp. 2019–2028, Dec. 2019.
[27] H. Zhou, W. Tao, C. Zhou, Y. Mao, G.-J. Li, and G. Liu, "Consequent pole permanent magnet Vernier machine with asymmetric air-gap field distribution," *IEEE Access*, vol. 7, pp. 109340–109348, 2019.
[28] H. Zhao, C. Liu, and Z. Song, "Design of an effective double-rotor machine with robust mechanical structure," *IEEE Trans. Magn.*, vol. 56, no. 1, pp. 1–7, Jan. 2020.
[29] Y. Li, Q. Zhou, J. Hang, W. Li, and S. Ding, "Investigation of torque contributions of main-order working harmonics in consequent-pole PM Vernier machines," in *Proc. IEEE 5th Int. Electr. Energy Conf. (CIEEC)*, May 2022, pp. 4853–4858.
[30] X. Ge, Z. Q. Zhu, J. Li, and J. Chen, "A spoke-type IPM machine with novel alternate airspace barriers and reduction of unipolar leakage flux by step-staggered rotor," *IEEE Trans. Ind. Appl.*, vol. 52, no. 6, pp. 4789–4797, Nov. 2016.
[31] Z. Q. Zhu, H. Hua, A. Pride, R. Deodhar, and T. Sasaki, "Analysis and reduction of unipolar leakage flux in series hybrid permanent-magnet variable flux memory machines," *IEEE Trans. Magn.*, vol. 53, no. 11, pp. 1–4, Nov. 2017.
[32] K. Wang, J. Li, S. S. Zhu, and C. Liu, "Novel hybrid-pole rotors for consequent-pole PM machines without unipolar leakage flux," *IEEE Trans. Ind. Electron.*, vol. 66, no. 9, pp. 6811–6823, Sep. 2019.
[33] S.-U. Chung, J.-W. Kim, B.-C. Woo, D.-K. Hong, J.-Y. Lee, and D.-H. Koo, "A novel design of modular three-phase permanent magnet Vernier machine with consequent pole rotor," *IEEE Trans. Magn.*, vol. 47, no. 10, pp. 4215–4218, Oct. 2011.
[34] L. Xu, Y. Li, W. Zhao, and G. Liu, "Reduction of unipolar leakage flux and torque ripple in consequent-pole PM Vernier machine," *CES Trans. Electr. Mach. Syst.*, vol. 7, no. 1, pp. 35–44, Mar. 2023.
[35] Y. Zheng, Z. Q. Zhu, D. Liang, Y. Zhou, H. Liu, and L. Chen, "Analysis and reduction of unipolar end leakage flux in consequent-pole Vernier and fractional slot PM machines," in *Proc. IEEE Int. Electric Mach. Drives Conf. (IEMDC)*, May 2023, pp. 1–7.
[36] J. Li, K. Wang, F. Li, S. S. Zhu, and C. Liu, "Elimination of even-order harmonics and unipolar leakage flux in consequent-pole PM machines by employing N-S-iron–S-N-iron rotor," *IEEE Trans. Ind. Electron.*, vol. 66, no. 3, pp. 1736–1747, Mar. 2019.
[37] J. Qi, Z.-Q. Zhu, L. Yan, G. W. Jewell, C. Gan, Y. Ren, S. Brockway, and C. Hilton, "Effect of pole shaping on torque characteristics of consequent pole PM machines," *IEEE Trans. Ind. Appl.*, vol. 58, no. 3, pp. 3511–3521, May 2022.
[38] Z. Q. Zhu, "A simple method for measuring cogging torque in permanent magnet machines," in *Proc. IEEE Power Energy Soc. Gen. Meeting*, Jul. 2009, pp. 1–4.

YINZHAO ZHENG received the B.Eng. degree in electrical engineering from Northwestern Polytechnical University, Xi'an, China, in 2017, and the M.Sc. degree in electrical engineering from Huazhong University of Science and Technology, Wuhan, China, in 2020. He is currently pursuing the Ph.D. degree with The University of Sheffield, Sheffield, U.K.

His major research interests include design optimization and thermal management of electrical machines.

ZI-QIANG ZHU (Fellow, IEEE) received the B.Eng. and M.Sc. degrees in electrical engineering from Zhejiang University, Hangzhou, China, in 1982 and 1984, respectively, and the Ph.D. degree in electronic and electrical engineering from The University of Sheffield, Sheffield, U.K., in 1991.

Since 1988, he has been with The University of Sheffield, where he currently holds the Royal Academy of Engineering/Siemens Research Chair and the Head of the Electrical Machines and Drives Research Group, the Academic Director of the Sheffield Siemens Gamesa Renewable Energy Research Centre, the Director of Sheffield CRRC Electric Drives Technology Research Centre, and the Director of Sheffield Midea Electrical Machines and Control Systems Research Centre. His research interests include the design and control of permanent-magnet brushless machines and drives for applications ranging from automotive through domestic appliances to renewable energy. He is a fellow of the Royal Academy of Engineering. He was a recipient of the 2021 IEEE Nikola Tesla Award and the 2019 IEEE IAS Outstanding Achievement Award.

HAI XU (Graduate Student Member, IEEE) received the B.Eng. and M.Sc. degrees in electrical engineering from Huazhong University of Science and Technology, Wuhan, China, in 2018 and 2021, respectively. He is currently pursuing the Ph.D. degree in electrical engineering with The University of Sheffield, Sheffield, U.K.

His current research interest includes the design and analysis of permanent magnet machines.

JUN YAN received the B.Eng. degree in electrical engineering from Hebei University of Science and Technology, Shijiazhuang, China, in 2019, and the M.Sc. degree in automation and control from Newcastle University, Newcastle upon Tyne, U.K., in 2020. He is currently pursuing the Ph.D. degree with The University of Sheffield, Sheffield, U.K.

His major research interests include position sensorless control and flux weakening control of permanent magnet synchronous machines and small-volume DC-link capacitor-based permanent magnet synchronous machine drives.

DAWEI LIANG (Member, IEEE) received the B.Eng. degree in electrical engineering from Harbin Institute of Technology, Harbin, China, in 2014, the M.Sc. degree in electrical engineering from Karlsruhe Institute of Technology, Karlsruhe, Germany, in 2018, and the Ph.D. degree in electrical engineering from The University of Sheffield, Sheffield, U.K., in 2022.

He is currently a Postdoctoral Research Associate with The University of Sheffield. His major research interests include thermal modeling and management, and parameter identification of electrical machines.